AGU PUBLICATIONS

JGR

Journal of Geophysical Research: Oceans

RESEARCH ARTICLE

10.1002/2015JC011026

# Do East Australian Current anticyclonic eddies leave the Tasman Sea?

**Gabriela S. Pilo[1,2], Peter R. Oke[2], Tatiana Rykova[2], Richard Coleman[1,3], and Ken Ridgway[2]**

[1]Institute for Marine and Antarctic Studies, University of Tasmania, Hobart, Tasmania, Australia, [2]CSIRO Oceans and Atmosphere Flagship, Hobart, Tasmania, Australia, [3]Antarctic Climate and Ecosystems CRC, Hobart, Tasmania, Australia

**Key Points:**
- EAC anticyclones propagate from the Tasman Sea toward the Indian Ocean
- EAC anticyclones decay along path and amplify due to merging with other eddies
- EAC anticyclones become more barotropic along their path

**Supporting Information:**
- Supporting Information S1

**Correspondence to:**
G. S. Pilo,
Gabriela.SemoliniPilo@utas.edu.au

**Citation:**
Pilo, G. S., P. R. Oke, T. Rykova, R. Coleman, and K. Ridgway (2015), Do East Australian Current anticyclonic eddies leave the Tasman Sea?, *J. Geophys. Res. Oceans*, *120*, 8099–8114, doi:10.1002/2015JC011026.

Received 8 JUN 2015
Accepted 16 NOV 2015
Accepted article online 19 NOV 2015
Published online 18 DEC 2015



**Abstract** Using satellite altimetry and high-resolution model output we analyze the pathway of large, long-lived anticyclonic eddies that originate near the East Australian Current (EAC) separation point. We show that 25–30% of these eddies propagate southward, around Tasmania, leave the Tasman Sea, and decay in the Great Australian Bight. This pathway has not been previously documented owing to poor satellite sampling off eastern Tasmania. As eddies propagate southward, they often "stall" for several months at near-constant latitude. Along the pathway eddies become increasingly barotropic. Eddy intensity is primarily influenced by merging with other eddies and a gradual decay otherwise. Surface temperature anomaly associated with anticyclonic eddies changes as they propagate, while surface salinity anomaly tends to remain relatively unchanged as they propagate.

## 1. Introduction

Ocean eddies play a critical role in the distribution of heat and other properties in the world's oceans [e.g., *Wunsch*, 1999; *Jayne and Marotzke*, 2002]. The most energetic eddies are found in western boundary current (WBC) regions [*Chelton et al*., 2011]. The East Australian Current (EAC) is the WBC of the South Pacific Subtropical Gyre. It is characterized by a warm, poleward current that flows as a jet between about 20–31°S off eastern Australia before separating from the coast at 31–32°S [*Godfrey et al*., 1980]. At this latitude band, the EAC retroflects and degenerates into a complex field of mesoscale eddies [e.g., *Nilsson and Cresswell*, 1980; *Ridgway and Godfrey*, 1997]. The EAC anticyclonic eddies form in the retroflection region (denoted in Figure 1) approximately every 90–100 days [e.g., *Bowen et al*., 2005; *Mata et al*., 2006]. These eddies have been shown to be important for the circulation, influencing the water mass distribution and transformation in the Tasman Sea, coastal upwelling [e.g., *Tranter et al*., 1982] and biological productivity [e.g., *Griffiths and Brandt*, 1983; *Baird et al*., 2011; *Everett et al*., 2012].

Previous analyses of EAC eddies indicate that they typically stay close to the continental slope between their formation region and about 40°S [*Everett et al*., 2012; *Pilo et al*., 2015]. However, some large anticyclonic eddies have also been identified off south-eastern Tasmania. For example, *Baird and Ridgway* [2012] and *Pilo et al*. [2015] show anticyclonic eddies, tracked in gridded altimetry, propagating from the Southern Tasman Sea region, crossing south of Tasmania, and advecting toward to the Great Australian Bight (GAB, Figure 1). We also note that the westward flow south of Tasmania is a component of the so-called Southern Ocean super-gyre, described by *Ridgway and Dunn* [2007]. This super-gyre is reported to include a continuous flow, on average, southward off south-eastern Australia, around the southern tip of Tasmania, and extending toward the Indian Ocean. These papers lead us to hypothesize that long-lived EAC eddies may follow this pathway. While it is agreed that EAC anticyclonic eddies propagate southward to about 40°S, the link between eddies shed by the EAC and eddies that propagate toward the GAB is unclear.

In this paper, we make a direct link between EAC anticyclonic eddies, that form in the EAC retroflection (~31°S) and leave the region, and anticyclonic eddies propagating toward the GAB (Figure 1, white line). Using data from an eddy-resolving, near-global ocean model and gridded sea level anomaly (SLA) maps, we manually track anticyclonic eddies that originate in the EAC retroflection and leave this formation region—and follow their evolution as they flow southward, adjacent to the continental slope, to the southern tip of Tasmania. This link between EAC eddies and eddies near the GAB has not been previously documented.

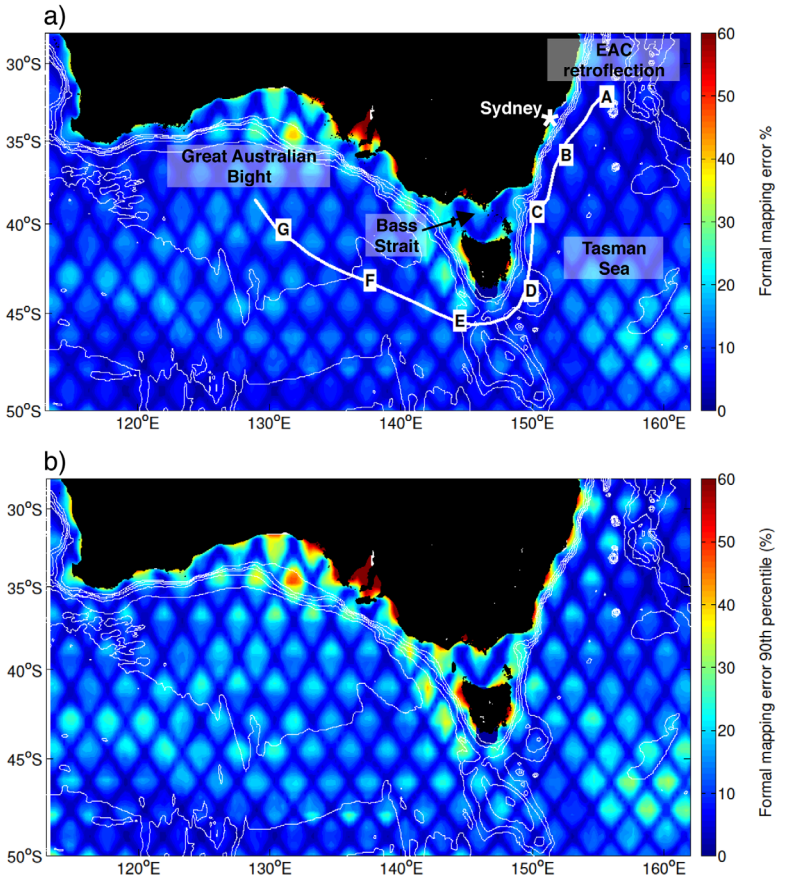


**Figure 1.** (a) Map of the time-averaged (1993–2012) and (b) 90th percentile formal mapping error, presented as a percentage of the signal variance, for the Aviso Reference Series SLA maps. White contours show topography from 1000 to 6000 m spaced every 1000 m. The thick white line denotes the eddy pathway that is discussed throughout this paper.

Details of the ocean model and observations used in this study are described in section 2, along with a description of our eddy-tracking method used here. Results are presented in section 3, where we look closely at the evolution of two ocean model eddies. Discussion and conclusions on our main findings are presented in section 4.

## 2. Data and Methods

### 2.1. Model

In this study, we use the output from the last 19 years of a 36 year run of the Ocean Forecasting Australian Model, version 3 (OFAM3) [*Oke et al.*, 2013]—a near-global eddy-resolving configuration of the GFDL Modular Ocean Model, version 4p1 [*Griffies et al.*, 2004]. The model has 1/10° horizontal grid spacing between 75°S and 75°N. The vertical grid is $z^*$, with 51 vertical levels, with 5 m spacing near the surface, 10 m spacing at 200 m depth, and coarser below that. OFAM3 is forced with 3 hourly surface heat, freshwater, and momentum fluxes from ERA-interim [*Dee and Uppala*, 2009], with restoring to monthly SST [*Reynolds et al.*, 2007, 10 day restoring time scale]; weak restoring to surface climatological salinity (180 day restoring) [*Ridgway and Dunn*, 2003]; and weak restoring to climatological temperature and salinity below 2000 m depth (restoring time scale of 180 days). *Oke et al.* [2013] provide a comprehensive description of all aspects of OFAM3, and show that the mean and variability of the model fields generally agree well with observations.

### 2.2. Observations

We supplement the analysis of the model fields with gridded SLA maps from two different products. We use SLA maps from the Aviso Reference Series (1/3° grid, 7 day maps using data from two altimeters [*Ducet et al.*, 2000]); and OceanCurrent (1/4° grid, 4 day maps using data from all available altimeters [*Deng et al.*,

2010]). We use OceanCurrent (an Australian data set produced by the Integrated Marine Observing System—IMOS) in addition to Aviso, because it has been extensively validated in the region of interest. Both Aviso and OceanCurrent use different versions of the same ~7 km resolution along-track altimetry (i.e., processed independently). The length scales used for the objective mapping range from 100 km in the zonal and meridional directions at 60°S–60°N, to 250 (350) km in the meridional (zonal) direction at the equator.

### 2.3. Limitations

Both the model and altimeter-based products used in this study have limitations. The model only represents a subset of the ocean variability. Horizontally, the model resolves features larger than ~50 km (five model grid points). Furthermore, the model has poor vertical resolution at depth, particularly below 2000 m, where temperature and salinity fields are restored to climatology [*Oke et al*., 2013]. For this reason, we restrict our analysis of the model fields to the top 2000 m. The model also has limitations associated with resolution and accuracy of surface forcing fields and topography. These limitations result in some systematic errors in the model, as described by *Oke et al*. [2013].

Although the altimetry gridded SLA fields are based on observations, they also have limitations. The altimeter products depend strongly on the assumed decorrelation length-scales and on the sampling of the altimeter tracks. For the Aviso Reference Series used here (i.e., maps produced by merging data from two satellites) the mapping error is below 10% of the signal variance for most of the study region (Figure 1a) [*Le Traon et al*., 1998], but can reach more than 25% of the signal variance (see the formal mapping error 90th percentile in Figure 1b). However, there are local maxima in the mapping error (Figure 1) that, as we will argue, have important implications for this study. The repeat cycle of different altimeters is between 10 and 35 days, and the average spacing between altimeter tracks in the merged product is about 40 km at midlatitudes. Consequently, it is reasonable to expect that the altimeter SLA maps do not reproduce all of the true mesoscale variability of the ocean. This means that analyses of the mesoscale ocean circulation based solely on SLA maps may sometimes be misleading. Indeed, the eddy pathway we identify in this study is not clear in gridded SLA fields or in SLA-derived products [e.g., *Chelton et al*., 2011]. We show that this lack of clarity in the observations is explained by relatively high mapping error at a key region along the identified EAC eddy pathway (e.g., off north-eastern and central-eastern Tasmania; see Figure 1). It is likely that this is why the eddy pathway we identify has not been previously documented.

### 2.4. Eddy Tracking

In this study, we track eddies manually. We chose this approach for two reasons. First, because we are analyzing only a small number of eddies we can afford to track each eddy carefully. This is crucial during complex "events," such as merging, observation gaps, and periods when the eddy becomes anisotropic. Second, the EAC is a challenging region for automated eddy-detection algorithms. Authors of different automated eddy-tracking methods [e.g., *Chaigneau et al*., 2008; *Chelton et al*., 2011] note that the algorithms are not perfect. Specifically, they note that such algorithms may perform poorly when eddies merge or when the flow field is particularly complex. We also note that manual tracking of features has a long history in atmospheric and meteorological research [e.g., *Hope et al*., 2014] and it has also been used to validate automatic eddy tracking in oceanographic research [e.g., *Chaigneau et al*., 2008; *Faghmous et al*., 2015]. However, even the manual tracking of eddies in this region was challenging—especially when using the observational products.

We recognize that manual tracking is somewhat subjective. To demonstrate the validity of the eddy tracks, we provide animations showing the evolution of modeled SLA fields for the study region and the tracked eddies using both modeled and observed fields (available online at http://www.youtube.com/GabrielaPilo).

In this study, we select anticyclonic eddies that form in the EAC retroflection region (~31°S). We track the selected eddy by locating closed positive SLA contours every 7 (OFAM3 and Aviso) or 4 (OceanCurrent) days. The center of the eddy is considered to be the location of the maximum positive SLA within the closed SLA contour. Consistent with the approach described by *Chelton et al*. [2011], we consider an eddy to be continuous in time if it is evident at consecutive time steps, with a tolerance of three time steps. That is, if the eddy is not clearly seen for three time steps, its trajectory is assumed to end.

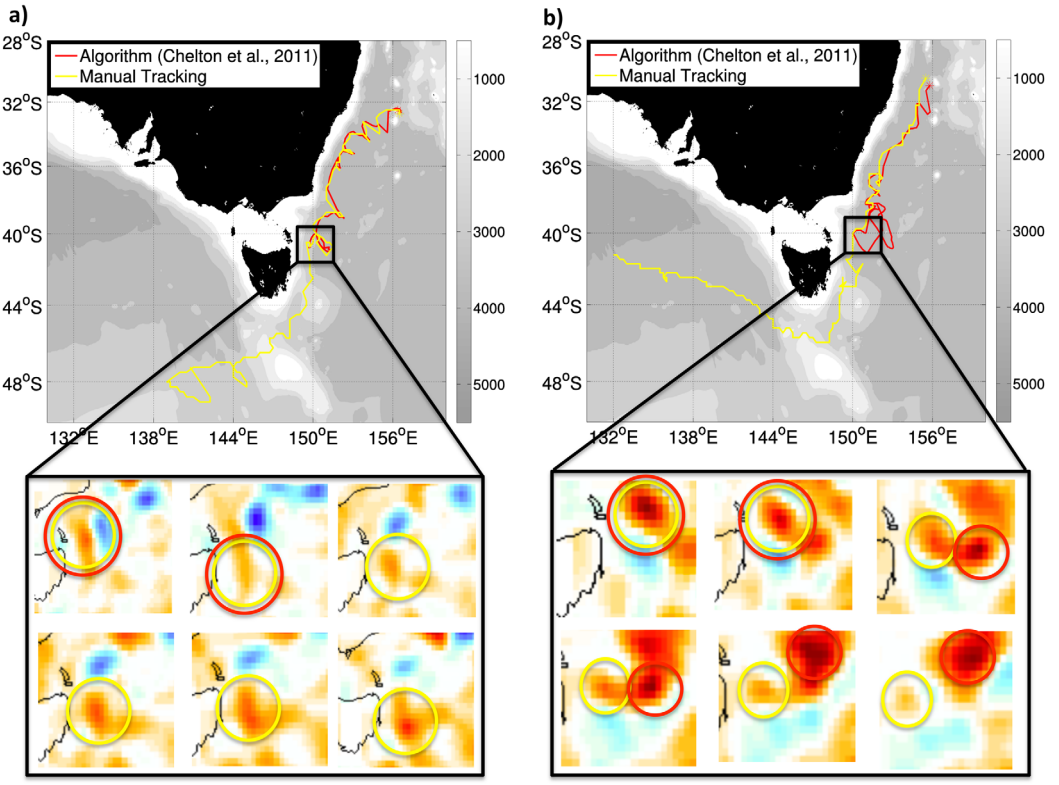


**Figure 2.** (a and b) Examples of eddy tracks using automated eddy detection (red) [*Chelton et al*., 2011] and manual tracking (yellow). Eddies were tracked in Aviso Reference Series sea level anomaly (SLA) gridded data sets. The bottom plots show a sequence of weekly SLA maps spanning the time when the tracks diverge; yellow (red) circles show the eddy perimeters from the manual (automatic) approach.

Eddies merge with other eddies as they propagate. In this study, we assume that if one eddy merges with another eddy its trajectory continues. This assumption is consistent with the observations described by *Cresswell* [1982], where two EAC anticyclonic eddies merged and the resulting eddy had the properties of the original eddies—with two layers of different water masses stacked at different depths.

In general, as the eddies propagate they lose energy and SLA decreases along their path. We track each eddy until its SLA becomes smaller than 0.05 m in OFAM3 and 0.1 m in Aviso and OceanCurrent. We use a larger threshold for the observational products because they have a smaller signal-to-noise ratio, mainly due to sampling error. By contrast, the model does not include noise due to sampling error. The eddy trajectory is also terminated if the eddy can no longer be identified as a closed SLA contour feature.

We have undertaken a comparison of eddy tracks using *Chelton et al.* [2011]'s Global Eddy Dataset version 3, and our manual tracking of eddies. Our comparisons with Chelton's database show cases when tracks end prematurely (e.g., Figure 2a; eddy #145708), or jump to an adjacent (different) eddy (e.g., Figure 2b; eddy #188703). The colored maps in Figure 2 show SLA around the time when the different tracking methods yield different results. In the first case (Figure 2a), the eddy changes its shape for 4 weeks and is no longer considered the same eddy by the automated eddy-detection algorithm. In the second case (Figure 2b), the tracked eddy approaches a different (larger) eddy, but the two eddies do not merge. The automated eddy-detection algorithm subsequently tracks the other eddy instead (red circles in SLA maps in Figure 2b). The manual approach continues tracking the original eddy as it continues southward (yellow circles in SLA maps in Figure 2b).

After manually tracking the eddies, we then extract all model fields at each time step (i.e., sea level and three-dimensional fields of temperature, salinity, and three components of velocity) for an 8° × 8° "box," centered on the eddy center. The eddy center is given by the local SLA maximum nearest the identified eddy location.

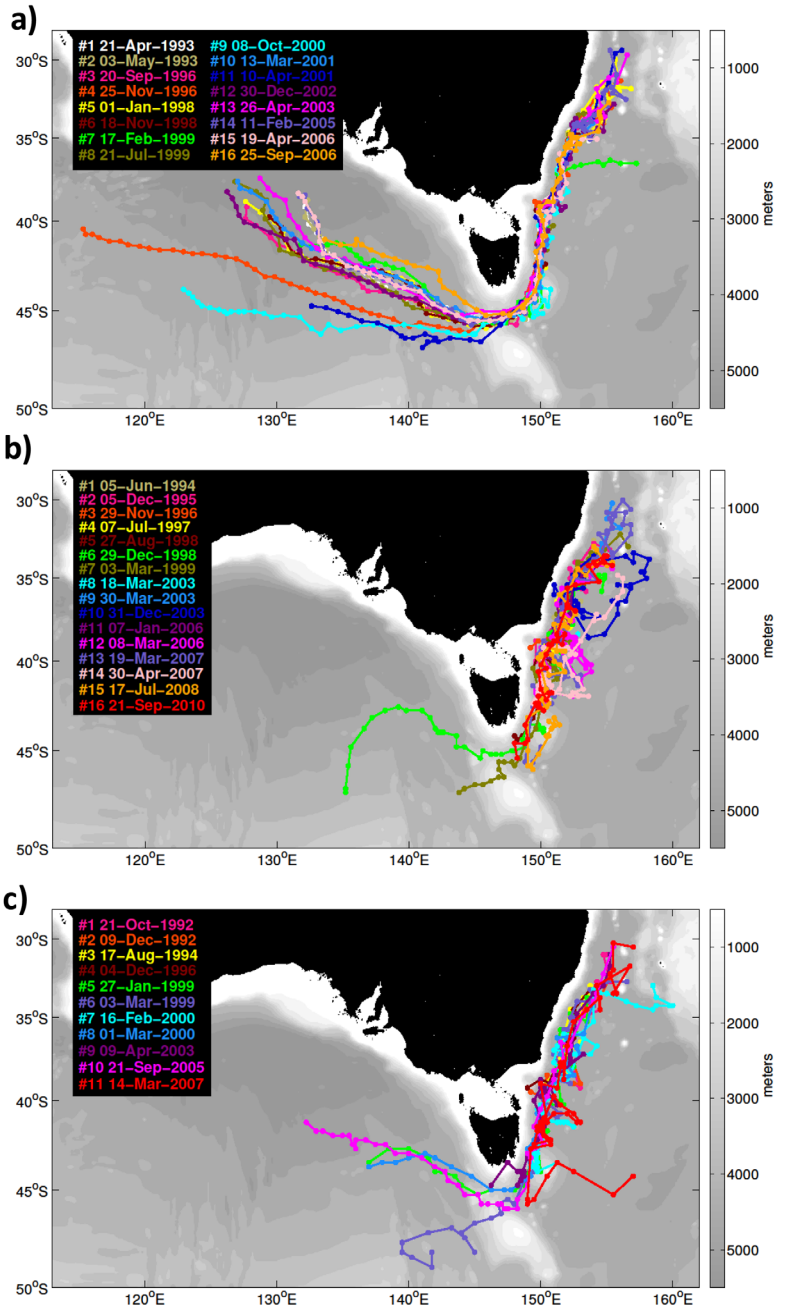


**Figure 3.** Tracks of anticyclonic eddies (colors) from (a) the model, (b) OceanCurrent, and (c) Aviso. Each eddy is identified in the legend by their start date. Gray shading denotes bathymetry and the dots along each path denote monthly time steps.

## 3. Results

### 3.1. Eddy Pathway

The tracks of the EAC anticyclonic eddies identified in the model and observations are displayed in Figure 3. In total, we track 16 eddies in the model, 16 eddies in OceanCurrent, and 11 eddies in Aviso. We find that many of the tracked eddies that leave the Tasman Sea follow a consistent pathway. This pathway begins in the EAC retroflection region, then extends southward, adjacent to the continental slope of south-eastern Australia, to the southern tip of Tasmania; and then continues toward the GAB. All 16 of the eddies tracked in the model roughly follow this pathway, 2 out of 16 eddies tracked in OceanCurrent, and 3 out of 11 eddies tracked in Aviso "survive" beyond Tasmania (i.e., only a 15–25% survival rate). We note that eddies

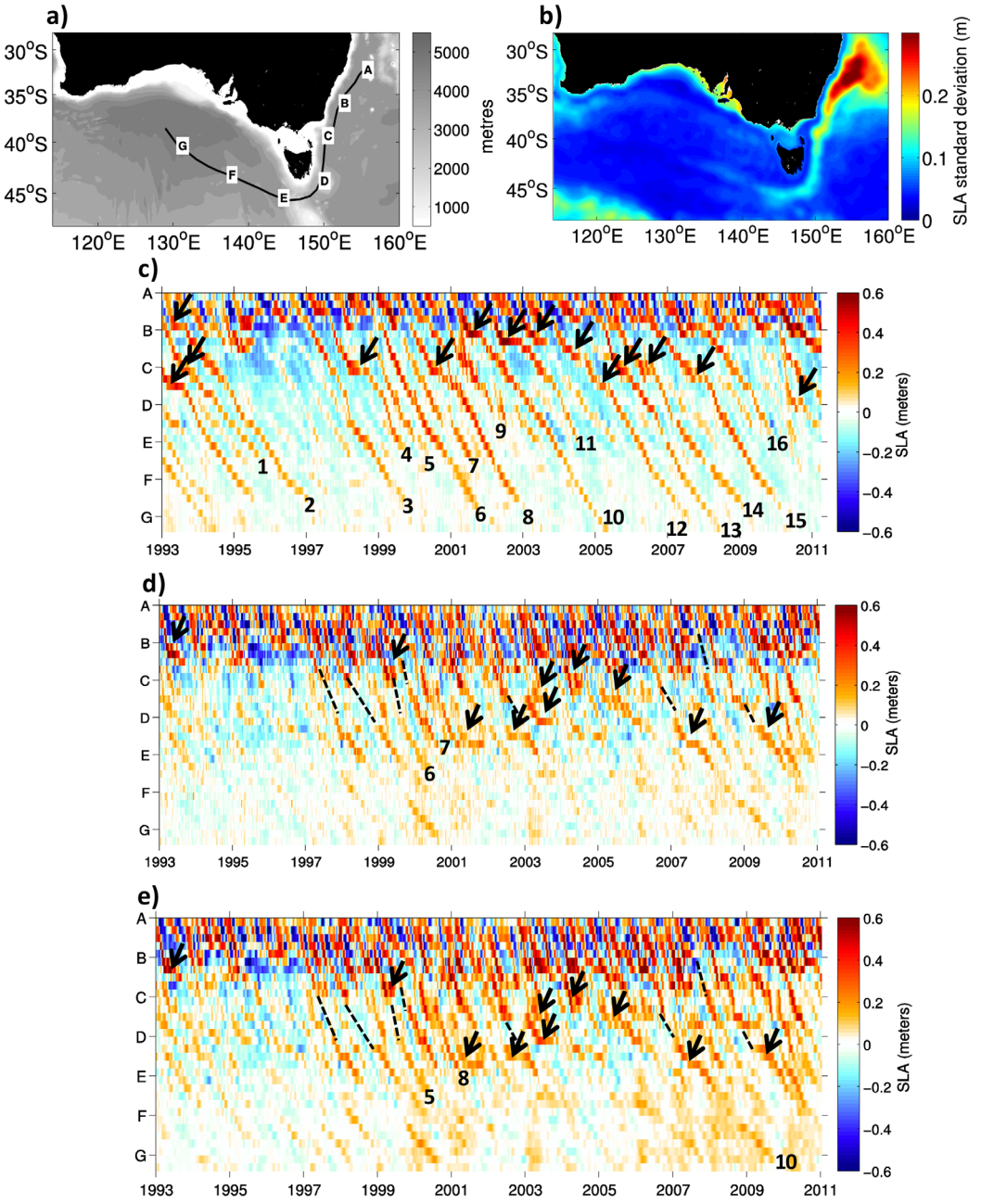


**Figure 4.** (a) Idealized pathway of anticyclonic eddies shed by the EAC retroflection in the model, overlaid on (a) bathymetry and (b) sea level anomaly (SLA) standard deviation from the model between 1993 and 2012 (colors). The letters (A to G) indicate key locations along the pathway. Hovmöller diagrams of SLA from (c) the model, (d) OceanCurrent, and (e) Aviso along A–G pathway with numbers relating to eddies from Figure 3; dashed lines indicate unresolved connections between observed eddies; black arrows denote moments when eddy propagation "stalls" along their path.

tracked in OceanCurrent and Aviso products are not always the same. This indicates that there are differences also between the observation-based products (due in part to different processing and number of altimeters used), and not only between the observations and the model.

To examine the temporal variability along the mean pathway—which is clearest in the model results (Figure 3a)—we produce Hovmöller diagrams of SLA from each data set along an idealized pathway (Figure 4). The idealized pathway (denoted A–G in Figure 4a) is not perfect, because the eddies do not always stay on this pathway (Figure 3). Despite this limitation, the evolution of positive SLAs along this idealized pathway is very clear in the model

**Table 1.** OFAM3 and Aviso Tracked Eddies' Mean Propagation Speed Between the EAC Retroflection Region and Off Sydney (A–B), Off Sydney and South of Tasmania (B–E), and at the Deep Basin South of Australia (E–G)[a]

| | A–B | B–E | E–G |
|---|---|---|---|
| OFAM3 | 5.5 ± 1.4 | 2.8 ± 0.4 | 3.2 ± 0.4 |
| Aviso | 8.0 ± 1.6 | 6.9 ± 1.4 | 3.6 ± 2.8 |

[a]Aviso's E–G section speed was calculated after four eddies only.

fields (Figure 4c), with all anomalies transiting beyond Tasmania, and 11 out of 16 making it to "G," along the pathway. These eddies take up to 5 years to complete their path.

Approximately 65–75 eddies are generated at the EAC retroflection region over a 19 year period [e.g., *Mata et al*., 2006]. However, not all these eddies leave the region, remaining there and interacting with other eddies [*Mata et al*., 2006]. In the model, 19 eddies formed in the EAC retroflection leave the Tasman Sea. Therefore, 25–30% of large anticyclonic eddies formed in the EAC retroflection leave the region and propagate southward, along the eddy pathway.

High SLA standard deviation values at the retroflection region are represented in the Hovmöller diagrams (Figure 4b; between "A" and "B"). Between these locations there is an alternance in cyclonic and anticyclonic eddies (negative and positive anomalies in Figures 4c–4e), indicating the high mesoscale activity.

The propagation of EAC anticyclonic eddies between "C" and "D" and beyond "E" is less clear in the observations (Figures 4d and 4e). However, we here suggest that eddies in the ocean do propagate along these paths—but, as they lose amplitude, their signal in the gridded products becomes less clear. Note that the section between C and D, in Figure 4a, spans a region where the mapping error is relatively high (between 20% and 25% of the signal variance and more than 25% in the 90th percentile; Figure 1). We denote (with black dashed lines in Figures 4c and 4d) several times when our analysis shows that eddies continue along the idealized pathway, despite a lack of signal in the gridded SLA in the observations. This is discussed further below.

Note that we do not expect an observed eddy to be evident in the model at the same time and location. This is because we are using fields from a "free" model run, with no data assimilation, and because eddy formation is somewhat chaotic. However, we do expect the model to generate eddies with realistic characteristics (size, shape, and amplitude), and we expect them to evolve in a manner consistent with observations (with a similar path, propagation speed, and time-evolution [*Oke et al*., 2008; *Schiller et al*., 2008; *Oke et al*., 2013]).

As part of their southward propagation many of the eddies "stall" at some point. These events are denoted by black arrows in Figures 4c–4e. In the model fields, the eddies often stall near "B" and "C" locations, off Sydney and off Bass Strait, respectively. In the gridded SLA fields, 3–4 eddies stall around Bass Strait, and 4–5 eddies stall off south-eastern Tasmania (with just one stalling near Sydney). These "stalling" events often last for several months when EAC anticyclonic eddies are quasi-stationary.

We can see differences in eddies propagation speeds when looking at OFAM3 and the altimetry Hovmöler diagrams (Figure 4). These different speeds are summarized in Table 1, indicating that the propagation speed of the observed and modeled eddies are comparable when they first form and as they propagate toward the GAB; but the observed eddies propagate about twice as fast as the model eddies as they move southward toward Tasmania. In part, the discrepancy between B and E is because the modeled eddies tend to "stall" for longer than the observed eddies. However, we note that the propagation speeds of the model eddies are consistent with other reports of eddy propagation speeds in this region from other observational studies [e.g., *Zhang et al*., 2014, see their Figure S2].

We noted above that several observed eddies moving along the idealized pathway appear discontinuous (see the dashed lines in Figures 4d and 4e). The location where the eddies "disappears" is often between "C" and "D," off eastern Tasmania (where the mapping error has a local maximum; Figure 1). We also note that the amplitude of the eddies when they "disappear" is small ($<$0.1 m), and hence close to the merged altimetry product resolution.

To test the altimetric sampling of the region off eastern Tasmania during periods of eddy transiting, we choose four eddies tracked in OceanCurrent gridded SLA maps (Figure 5). Two examples (Figures 5a and 5b) show cases when there is poor altimetric sampling and the eddies "disappear" in the region of relatively high mapping error (Figure 1). Two examples (Figures 5c and 5d) show cases when there is good altimetric

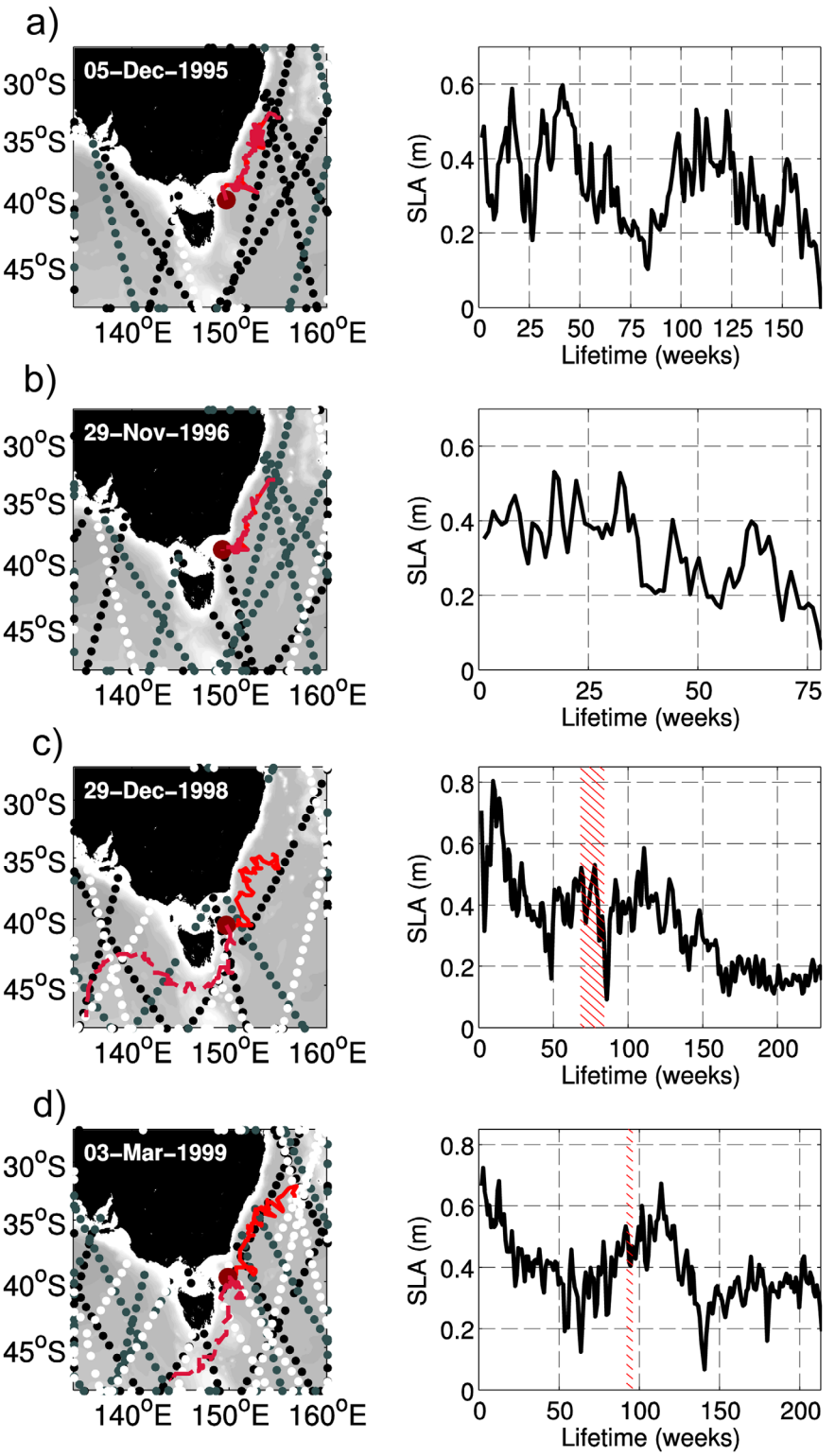


**Figure 5.** Maps of tracked eddies from OceanCurrent (left plots, red lines). The left plots in row show tracks that (a and b) end off Bass Strait and (c and d) extend beyond Tasmania. The dots show data points along altimeter tracks when eddies are off Bass Strait (time *t*). Black, gray and white dots denote times $t-2$, $t-1$, and *t*, respectively. The right plots show times series of sea level anomalies for each eddy. The hatched region indicates proximity to Bass Strait slope.

sampling and the eddy pathway continues beyond Tasmania. We show that eddies that dissipate (i.e., "disappear") off Bass Strait were under-sampled. Also, due to their reduced SLA (plots in Figure 5, showing SLA ~5 cm) they are not well resolved in the SLA gridding process, which has comparable errors (~5 cm). Therefore, we attribute this "disappearance" to relatively high mapping error and poor altimetric sampling of the region off eastern Tasmania during periods of eddy transit (see Figures 1 and 5).

The fact that the Hovmöller diagrams (Figures 4d and 4e) show these eddies "reappearing" at about the right time (assuming approximately steady southward propagation; see dashed lines) suggests that indeed the true eddies do regularly transit along the pathway. However, the gridded SLA altimetry fields do a relatively poor job of capturing this variability.

### 3.2. Eddy Evolution

To examine the temporal variability of sea surface properties along the mean pathway we produce Hovmöller diagrams of Sea Surface Temperature (SST; Figure 6), Sea Surface Salinity (SSS; Figure 7), and their anomalies (SSTA and SSSA) from the model along the idealized pathway.

A SST front between warm tropical waters from the Coral Sea (>22°C) and cold temperate waters from the Tasman Sea (<10°C) occurs in the region of interest (Figure 6a). The mean location of this front is at 40°S, extending further south off the eastern Australia coast, due to advection of warmer waters by the EAC and its eddies. Therefore, eddies propagating along the pathway are formed in warmer regions and propagate toward colder regions. The SSTA standard deviation displays higher values close to the EAC retroflection and southeast of Tasmania (Figure 6b). Here the seasonal signal was removed, therefore this variability is mainly attributed to local mesoscale variability.

The evolution of SST along the pathway has a strong seasonal signal (Figure 6c). This signal hinders the observation of eddies propagation on the SST Hovmöller diagram. Despite this hindering, it is possible to see the SST signature of the eddies previously seen in the model SLA Hovmöller diagram (Figure 4b) propagating along the pathway. With the seasonal signal removed, the SSTA associated with the eddies is clearer (Figure 6d). Due to their warm-core nature, EAC anticyclonic eddies are seen as a positive SSTA. Although less persistent than the eddies' positive SLA (Figure 4c), positive SSTA can be tracked as far as "F," off western Tasmania, in most cases (e.g., eddies 2, 3, 6, 8, 10, 12, 13).

A SSS front between saltier tropical waters from the Coral Sea (>35.6 psu) and fresh temperate waters from the Tasman Sea (<35 psu) occurs in this region (Figure 7a). The mean location of this front is at 40°S, extending further south off eastern Australia coast toward Tasmania. The eddy pathway transits through different SSS values, encountering saltier waters of the EAC and fresher waters south of Australia. The standard deviation of SSSA displays higher values close to the EAC retroflection, south of Tasmania and south of Western Australia (Figure 7b). This variability is not attributed to a seasonal signal. At the EAC retroflection, this variability can be explained by the variable location of the EAC itself. South of Tasmania, this variability can be explained by movements of the subtropical convergence [*Wyrtki*, 1960; *Ridgway and Dunn*, 2003].

The evolution of SSS along the pathway has no strong seasonal signal (Figure 7c). In this case, the salinity differences between the Coral and the Tasman Seas (between "C" and "D" in the SSS Hovmöller diagram) are the very clear. Even with this strong signal, the signature of the eddies' propagation along the pathway is evident. The saltier EAC water entrained by the eddies during their formation is retained along the entire pathway. Consideration of seasonal anomalies of SSS yields a clearer picture of the eddy propagation along the pathway (Figure 7d). However, after the "D" location we see a misleading increase in SSSA. This increase does not represent an increase in eddies' SSS, but a higher SSSA due to the eddy propagating along a highly variable region (Figure 7b).

#### 3.2.1. Case Studies

The Hovmöller diagrams (Figures 4c–4e) show that eddies' surface signals fluctuates with time. The eddies' SLA signal often slowly decreases as the eddies propagate, and sometimes increases over just a few weeks, both in the model and the observations. To better understand this, we present two detailed descriptions of model eddies, hereafter Eddy #3 and Eddy #9. These eddies are representative of the sample of model eddies included in this study (the same details for all model eddies are included in supporting information Figures S1–S14).

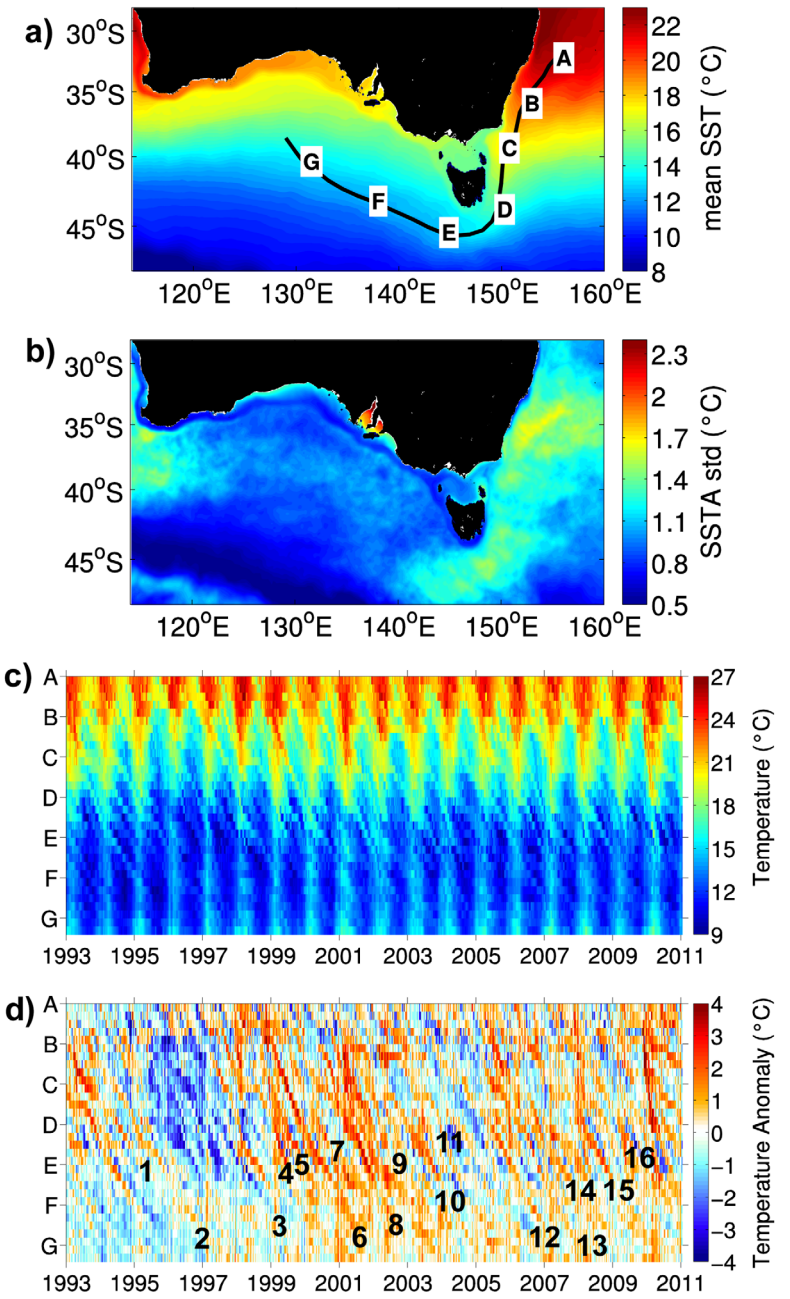


**Figure 6.** Eddies' surface temperature evolution; (a) idealized pathway of anticyclonic eddies shed by the EAC retroflection in the model, overlaid on mean sea surface temperature (SST) from the model between 1993 and 2012. The letters (A–G) indicate key locations along the pathway; (b) map of SST Anomaly (SSTA) standard deviation from the model between 1993 and 2012; (c) Hovmöller diagram of SST from the model along A–G pathway; (d) as for Figure 6c, but for SSTA with numbers relating to eddies from Figure 3a.

Here we show various eddy characteristics, including their amplitude, horizontal velocity vertical profile, and barotropic-baroclinic partitioning, as the eddies propagate along the pathway. To quantify the barotropic-baroclinic partitioning of the eddies as they evolve, we compute the normal vertical modes along their path (Figure 8c). This is achieved by solving the Sturm-Liouville eigenvalue problem [e.g., *Wunsch*, 1997; *Venaille et al*., 2011], using the Coriolis parameter and profiles of velocity and the buoyancy frequency. At each time step, we use an average profile that is midway between the eddy center and the edge of the eddy to the east—usually about 100 km east of the eddy center. We then compute the ratio of the first and second eigenvalue to the sum of all eigenvalues, quantifying the percentage of the velocity profile that projects onto the zeroth mode (the barotropic mode) and the first baroclinic mode. Sensitivity

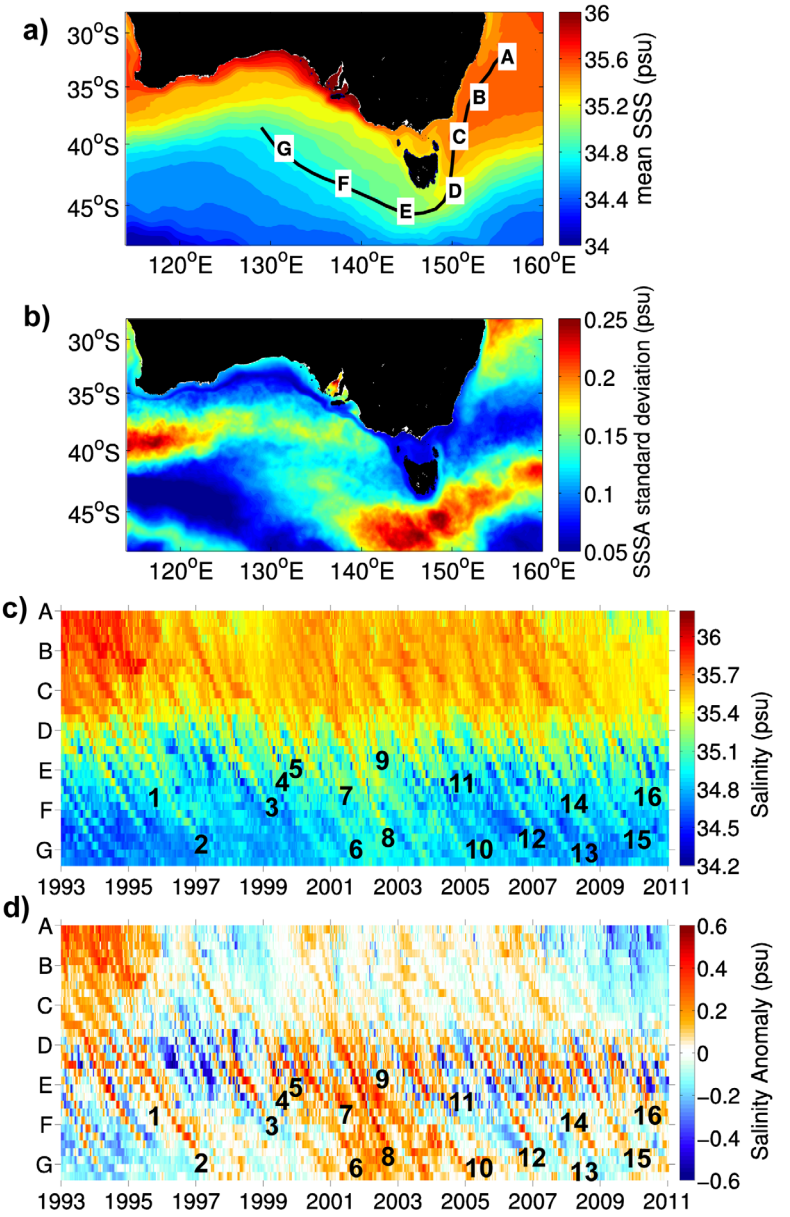


**Figure 7.** Eddies' surface salinity evolution; (a) as for Figure 6a, but for Sea Surface Salinity (SSS); (b) as for Figure 6b, but for SSS Anomaly (SSSA); (c) as for Figure 6c, but for SSS; (d) as for Figure 6d, but for SSSA.

tests indicate no significant difference when using average profiles on the eastern or western side of each eddy.

### 3.2.2. First Case Study: Eddy #3

Eddy #3's SLA changes as the eddy propagates (Figure 8a). When the eddy is between the EAC retroflection region ("A") and southeast of Tasmania ("D") the SLA varies between 0.17 and 0.45 m. SLA increases sharply after eddy merging events (red lines between "A" and "D"), but slowly decrease otherwise. After the eddy propagates beyond Tasmania the SLA decays, reaching ∼0.1 m before dissipating completely.

The eddy's horizontal velocity vertical profile also changes as it propagates along the pathway. To demonstrate that, we show snapshots of Eddy #3 immediately after it forms (Figure 8b, left), when it is located off Bass Strait (Figure 8b, middle), and when it propagates toward the GAB (Figure 8b, right). Immediately after formation the velocity field is surface-intensified with values of over 1 m/s, with moderate velocities penetrating to depths of about 1800 m, and with strong vertical shear—characteristic of a strongly baroclinic

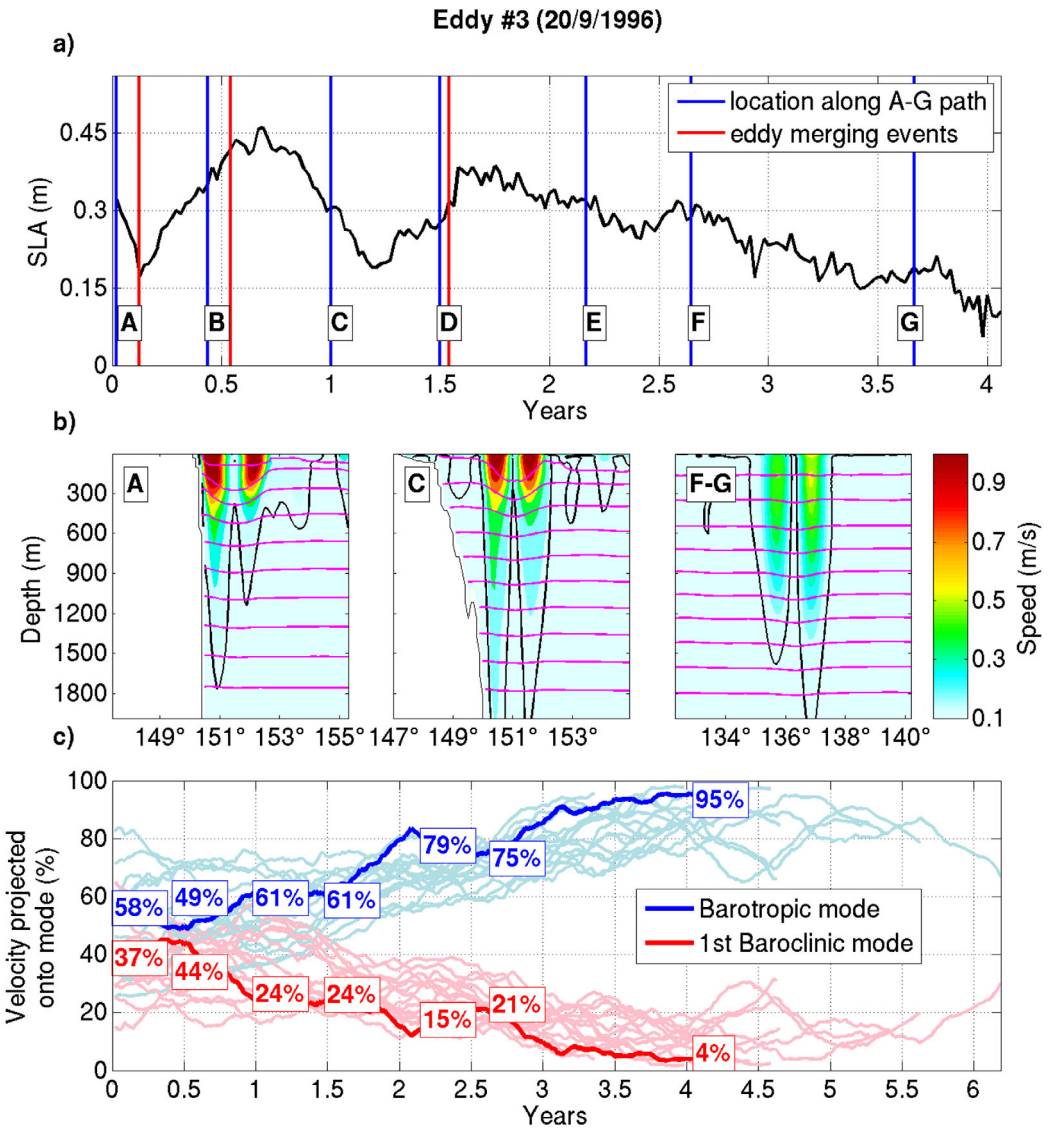


**Figure 8.** (a) Times series of SLA at the center of Eddy #3; (b) snapshots of velocity (color; black contour denoting 0.1 cm/s) and potential density (magenta contours; contour intervals are 0.1 kg/m$^3$) near "A," "C," and "F–G" locations; and (c) time series of the percentage of velocity that projects onto the barotropic (blue) and first baroclinic (red) modes for Eddy #3 (bold lines) and for all other model eddies (thin lines). The percentages at each point, "A–G," are denoted in boxes. Note that axes in subplots a and c are different.

flow. By the time Eddy #3 propagates to Bass Strait, it has weaker surface velocity, when compared to its formation period. The eddy still shows deep penetration of the velocities (over 2000 m), and weakening vertical shear. The eddy velocity is much weaker by the time it reaches the GAB, and is characterized by a velocity field that shows weak vertical shear—characteristic of a quasi-barotropic flow. Note that the maximum velocities are subsurface at "F-G"—centered around 200 m depth.

The velocity profiles suggest that the eddy is more baroclinic when it first forms, and becomes more barotropic as it propagates along the pathway. Low-pass filtered time series of the ratio of eigenvalues, quantifying the barotropic-baroclinic partitioning, are shown in Figure 8c, with results for Eddy #3 (bold lines) and for all other eddies (thin lines). The results in Figure 8c quantify what is evident in Figure 8b—namely that Eddy #3 becomes more barotropic along its path, with 58% of the velocity explained by the barotropic mode when the eddy forms, increasing to 95% as it approaches the GAB. Conversely, the percentage of the velocity field projecting onto the first baroclinic mode decreases from 37%, when Eddy #3 first forms, to 4% as it reaches the GAB.

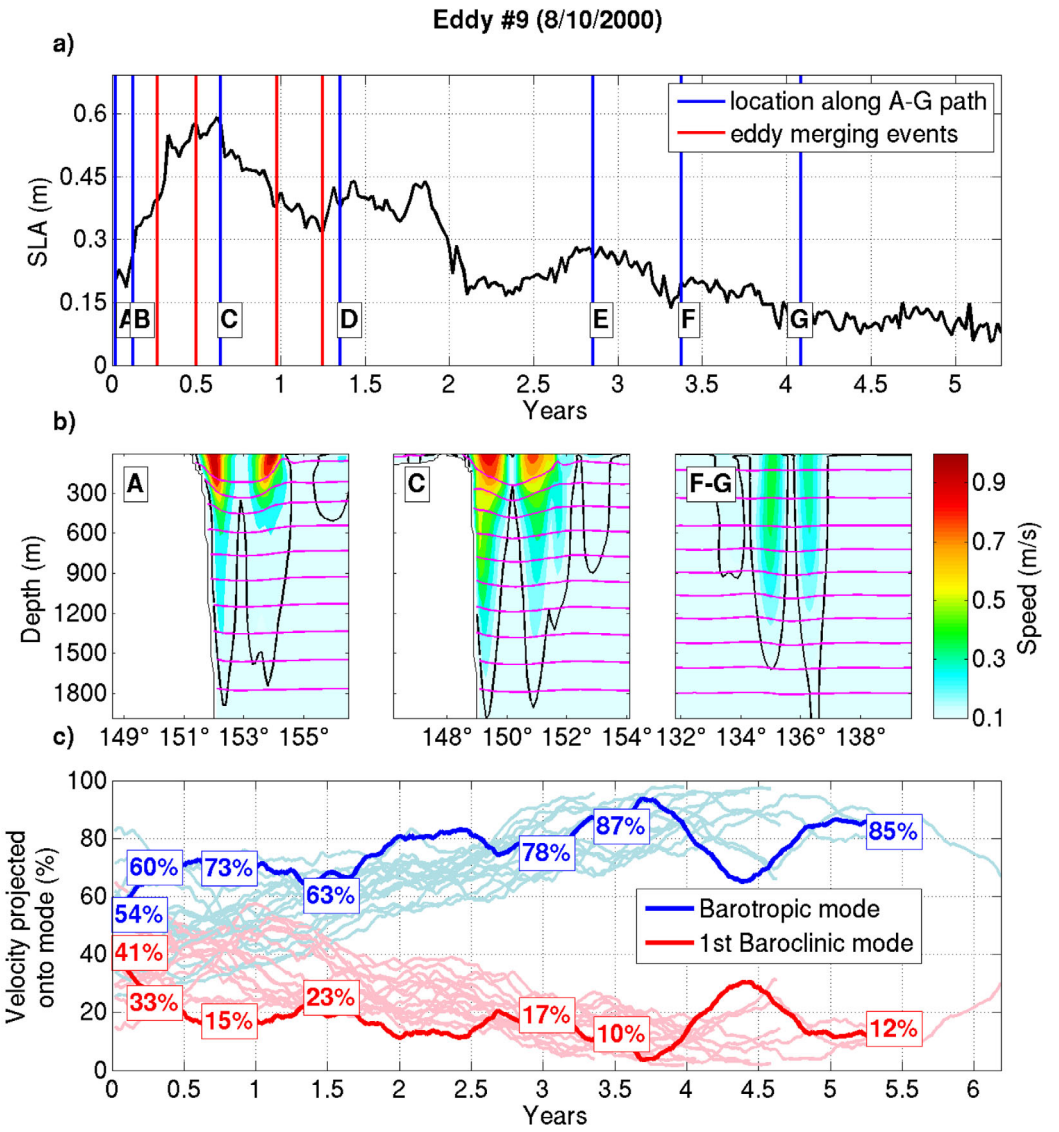


**Figure 9.** As in Figure 8, but for Eddy #9.

### 3.2.3. Second Case Study: Eddy #9

Eddy #9's SLA changes as the eddy propagates (Figure 9). Here on one merging event, there was no increase in eddy SLA. Similar to Eddy #3, the SLA varies between the EAC retroflection ("A") and southeast of Tasmania ("D"), decreasing almost monotonically when the eddy is propagating toward the GAB (i.e., after "E").

This eddy's vertical velocity profile also changes as it propagates along the pathway. Immediately after formation (Figure 9b, left) the velocity field is surface-intensified with values of ~0.8 m/s, with lower velocities penetrating deeper than 1800 m. The velocity profile for Eddy #9 is more asymmetric than for Eddy #3, with larger velocities penetrating deeper on its western flank. We believe this asymmetry to be caused by the eddy interaction with the continental slope, and further studies on this matter are underway. By the time Eddy #9 propagates to Bass Strait, it has weaker surface velocity when compared to its formation period. The eddy still shows deep penetration of the velocities (over 2000 m), and a much weaker vertical shear. The eddy velocity, as its vertical shear, is much weaker by the time it reaches the GAB. Here the maximum velocities are also subsurface—centered around 300 m depth.

Eddy #9 becomes more barotropic along its path, with 54% of the velocity explained by the barotropic mode when the eddy forms, increasing to ~80% before the eddy dissipates. Conversely, the percentage of

the velocity field projecting onto the first baroclinic mode decreases from 41%, when Eddy #9 first forms, to ~15% before the eddy dissipates.

From these two case studies (and also the eddies shown in the supporting information), we conclude that it is common for an eddy to merge at least 3 times along its path, with most merging events occurring in the Tasman Sea (before "D" in Figure 4). During merging events the SLA typically increases by 0.05–0.25 m. In between merging events, and after the eddy propagates beyond Tasmania, it is typical for an eddy to slowly decrease in amplitude, primarily owing to the loss of energy [e.g., *Flierl*, 1984; *Qiu et al*., 1997; *McDonald*, 1998].

## 4. Discussion and Conclusions

In this study, we show that EAC long-lived anticyclonic eddies mostly follow a consistent pathway and leave the Tasman Sea. Specifically, we find that ~25–30% of anticyclonic eddies that form in the EAC retroflection region propagate southward, adjacent to the continental slope, and transit south of Tasmania. Besides advection by the EAC extension, *Shi and Nof* [1994] suggest that the "image effect" can be the driver for the propagation of EAC anticyclonic eddies southward. After crossing south of Tasmania, the eddies propagate west-north-westward, toward the GAB. This part of the pathway is consistent with the existing literature [*Ridgway and Dunn*, 2007; *Baird et al*., 2011]. The west-north-westward propagation is also consistent with previous reports of anticyclonic eddy paths in other regions [e.g., *Morrow*, 2004; *Chelton et al*., 2011]. Based on our analysis, we suggest that most EAC anticyclonic eddies that follow the identified pathway finally decay in the deep basin south of the GAB. However, *Cresswell and Peterson* [1993] sampled an anticyclonic eddy off the southern tip of Western Australia (~177°E) carrying Bass Strait waters. Their observations imply that some eddies have propagated further northwest, well beyond the pathway identified in our study.

The interaction between eddies and the mean flow has been extensively studied in Northern Hemisphere WBCs [e.g., *Waterman and Jayne*, 2011, and references therein], and in the Agulhas Current [e.g., *Biastoch and Krauss*, 1999; *de Ruijter et al*., 1999], and to a smaller extent in the Brazil Current [*Oliveira et al*., 2009; *Rocha et al*., 2014] and in the East Australian Current [*Bowen et al*., 2005; *Mata et al*., 2006]. Within the EAC region, eddies might regulate the local recirculation where the current separates from the coast [*Mata et al*., 2006].

In the EAC retroflection, newly formed eddies can either coalesce with the EAC [*Nilsson and Cresswell*, 1980] or grow and leave the region [*Mata et al*., 2006; *Everett et al*., 2012; *Pilo et al*., 2015]. EAC anticyclonic eddies that coalesce with the EAC lose barotropic energy to the mean flow [*Mata et al*., 2006]. EAC anticyclonic eddies that grow and leave the region receive both baroclinic and barotropic energy from the mean flow [*Bowen et al*., 2005; *Mata et al*., 2006]. As the eddies move southward their baroclinic energy is lost back to the mean flow [*Mata et al*., 2006]. Our results are consistent with this energy loss in Figures 8 and 9, where eddies slowly decay after leaving the EAC retroflection and become less baroclinic as they propagate along the pathway. Exceptions to this slow eddy decay occur during eddy merging events, as shown here, and during eddy interactions with other local instabilities [*Mata et al*., 2006]. The interaction between eddies and the mean flow is clearly important to EAC eddies, their evolution, and propagation. We plan to study the energetics of these interactions in the future.

We find that the SLA amplitude of these eddies fluctuates along the pathway. The primary cause of these fluctuations is merging with other eddies. Typically, a merging event results in an increase in the maximum SLA. In the absence of any merging events, the amplitude of the eddies gradually decrease, as expected [*Flierl*, 1984; *Qiu et al*., 1997; *McDonald*, 1998]. We note that some of the eddies decay faster if they "stall" off Bass Strait. During those periods, the eddies often "push up" against the continental slope, remaining at a near-constant latitude for several months. We hypothesize that these eddies encounter stronger than usual bottom stress on the continental slope, explaining their enhanced decrease in amplitude. This "stalling" behavior has been previously reported by *Nilsson et al*. [1977]. The authors sampled one anticyclonic eddy off New South Wales (~35°S) that remains in the same region for 7 weeks. The volume of that eddy decreased by 10–30% during the stalling period. We are investigating changes in eddy amplitude and volume during "stalling" in more detail in another study.

While the SSTA signature of the eddies change as they propagate, decreasing in eddies' later life stages, the SSSA signature of the eddies persists along the pathway. The eddies' SSTA signature, although present, is weak. This weakness can be attributed to vertical mixing with cooler Tasman Sea waters, surface heat loss,

capping [*Tranter et al*., 1980; *Cresswell and Legeckis*, 1986] and flooding effects [*Tranter et al*., 1982; *Baird et al*., 2011]. In the later stages of eddies' "lives" the SSTA is almost absent, when compared to the SLA signature. This may be due to the eddies' tendency to have a subsurface core during these final stages (Figures 8 and 9). The eddies' SSSA signal persists as eddies propagate along the pathway. Our SSSA Hovmöler diagram (Figure 7d) shows a freshening of waters close to the EAC retroflection ("A" location), as also seen in Argo floats data [*Rykova and Oke*, 2015].

Consideration of Hovmöller diagrams of different variables (Figures 4c, 6d, and 7d) reveals a different pattern between 1995 and 1997. During this period no eddies propagate along the pathway. Also, there are smaller values of SLA, SSTA, and SSSA when compared to post-1997 years. The 1995–1997 period is associated with a reduced southward EAC transport and increased eastward Tasman Front transport [*Ridgway et al*., 2008; *Hill et al*., 2011]. We expect that a weaker EAC transport may lead to fewer eddies being shed and a smaller magnitude of SSTA and SSSA in that region.

We find that altimetry sampling is problematic off eastern Tasmania (Figure 1). There are relatively long periods when no altimeter tracks cross the described eddy pathway, resulting in a local maximum in the mapping error of the gridded SLA (see Figure 1). As a result, this identified eddy pathway has not been documented previously. This study, instead, made use of an eddy-resolving ocean model output (which of course is imperfect, but has sufficient spatiotemporal coverage for studies of mesoscale variability) to complement the analysis of observation-based gridded SLA fields. This allowed us to see the eddy pathway more clearly.

The EAC anticyclonic eddy pathway shown here provides a direct connection, albeit over several years, between the EAC retroflection region and the GAB. Thus, it allows for advection of EAC waters well beyond the Tasman Sea. As the eddies propagate southward, they interact with different regions along the Australian continental shelf break. This interaction can lead to local changes in ocean temperature and biogeochemistry, that ultimately affect habitat conditions for the marine biota.

**Acknowledgments**

Gabriela S. Pilo acknowledges support by the CAPES Foundation, Brazilian Ministry of Education (grant 0520-13-6). The authors gratefully acknowledge input from Maxim Nikurashin, that led to improvements in this work, and the comments from both anonymous reviewers. The Reference Series' Aviso altimeter products were produced by Ssalto/Duacs and distributed by Aviso, with support from Cnes (http://www.aviso.altimetry.fr/duacs, downloaded in September/2013). The Ocean Current altimeter products were produced by CSIRO and distributed by the Integrated Marine Observing System (http://oceancurrent.imos.org.au, downloaded in February/2014). OFAM3 was developed under Bluelink: a partnership between CSIRO, the Bureau of Meteorology, and the Royal Australian Navy (http://wp.csiro.au/bluelink/, downloaded in January/2014). The global eddy data set was developed and made freely available by D. Chelton and M. Schlax (cioss.coas.oregonstate.edu/eddies/, downloaded in December/2011).

## References

Baird, M. E., and K. R. Ridgway (2012), The southward transport of sub-mesoscale lenses of Bass Strait Water in the centre of anti-cyclonic mesoscale eddies, *Geophys. Res. Lett.*, *39*, L02603, doi:10.1029/2011GL050643.

Baird, M. E., I. M. Suthers, D. A. Griffin, B. Hollings, C. Pattiaratchi, J. D. Everett, M. Roughan, K. Oubelkheir, and M. Doblin (2011), The effect of surface flooding on the physicalbiogeochemical dynamics of a warm-core eddy off southeast Australia, *Deep Sea Res., Part II*, *58*(5), 592–605, doi:10.1016/j.dsr2.2010.10.002.

Biastoch, A., and W. Krauss (1999), The role of mesoscale eddies in the source regions of the Agulhas Current, *J. Phys. Oceanogr.*, *29*(9), 2303–2317, doi:10.1175/1520-0485(1999)029<2303:TROMEI>2.0.CO;2.

Bowen, M. M., J. L. Wilkin, and W. J. Emery (2005), Variability and forcing of the East Australian Current, *J. Geophys. Res.*, *110*, C03019, doi:10.1029/2004JC002533.

Chaigneau, A., A. Gizolme, and C. Grados (2008), Mesoscale eddies off Peru in altimeter records: Identification algorithms and eddy spatio-temporal patterns, *Prog. Oceanogr.*, *79*(2–4), 106–119, doi:10.1016/j.pocean.2008.10.013.

Chelton, D. B., M. G. Schlax, and R. M. Samelson (2011), Global observations of nonlinear mesoscale eddies, *Prog. Oceanogr.*, *91*(2), 167–216, doi:10.1016/j.pocean.2011.01.002.

Cresswell, G. R. (1982), The coalescence of two East Australian current warm-core eddies, *Science*, *215*(4529), 161–164, doi:10.1126/science.215.4529.161.

Cresswell, G. R., and R. Legeckis (1986), Eddies off southeastern Australia, *Deep Sea Res., Part A*, *33*(11/12), 1527–1562, doi:10.1016/0198-0149(86)90066-X.

Cresswell, G. R., and J. Peterson (1993), The Leeuwin Current south of Western Australia, *Aust. J. Mar. Freshwater Res.*, *44*(2), 285–303, doi:10.1071/MF9930285.

Dee, D. P., and S. Uppala (2009), Variational bias correction of satellite radiance data in the ERA-interim reanalysis, *Q. J. R. Meteorol. Soc.*, *135*(644), 1830–1841, doi:10.1002/qj.493.

Deng, X., D. A. Griffin, K. Ridgway, J. A. C. W. E. Featherstone, N. J. White, and M. Cahill (2010), Satellite altimetry for geodetic, oceanographic and climate studies in the Australian region, in *Coastal Altimetry*, edited by P. C. S. Vignudelli, A. G. Kostianoy, and J. Benveniste, pp. 473–508, Springer, Berlin.

de Ruijter, W. P. M., P. J. van Leeuwen, and J. R. E. Lutjeharms (1999), Generation and evolution of natal pulses: Solitary meanders in the Agulhas current, *J. Phys. Oceanogr.*, *29*(12), 3043–3055, doi:10.1175/1520-0485(1999)029<3043:GAEONP>2.0.CO;2.

Ducet, N., P. Y. Le Traon, and G. Reverdin (2000), Global high-resolution mapping of ocean circulation from TOPEX/Poseidon and ERS-1 and −2, *J. Geophys. Res.*, *105*(C8), 19,477–19,498, doi:10.1029/2000JC900063.

Everett, J. D., M. E. Baird, P. R. Oke, and I. M. Suthers (2012), An avenue of eddies: Quantifying the biophysical properties of mesoscale eddies in the Tasman Sea, *Geophys. Res. Lett.*, *39*, L16608, doi:10.1029/2012GL053091.

Faghmous, J. H., I. Frenger, Y. Yao, R. Warmka, A. Lindell, and V. Kumar (2015), A daily global mesoscale ocean eddy dataset from satellite altimetry, *Sci. Data*, *2*, 150028, doi:10.1038/sdata.2015.28.

Flierl, G. R. (1984), Rossby wave radiation from a strongly nonlinear warm eddy, *J. Phys. Oceanogr.*, *14*, 47–58.

Godfrey, J. S., G. R. Cresswell, T. J. Golding, A. F. Pearce, and R. Boyd (1980), The separation of the East Australian Current, *J. Phys. Oceanogr.*, *10*(3), 430–440, doi:10.1175/1520-0485(1980)010<0430:TSOTEA>2.0.CO;2.

Griffies, S. M., M. L. Harrison, R. C. Pacanowski, and A. Rosati (2004), A technical guide to MOM4, *GFDL Ocean Group Tech. Rep. 5*, NOAA/Geophys. Fluid Dyn. Lab. [Available at www.gfdl.noaa.gov.]
Griffiths, F., and S. Brandt (1983), Mesopelagic crustacea in and around a warm-core eddy in the Tasman Sea off eastern Australia, *Aust J. Mar. Freshwater Res.*, *34*(4), 609–623, doi:10.1071/MF9830609.
Hill, K. L., S. R. Rintoul, K. R. Ridgway, and P. R. Oke (2011), Decadal changes in the South Pacific western boundary current system revealed in observations and ocean state estimates, *J. Geophys. Res.*, *116*, C01009, doi:10.1029/2009JC005926.
Hope, P., K. Keay, M. Pook, J. Catto, I. Simmonds, G. Mills, P. McIntosh, J. Risbey, and G. Berry (2014), A comparison of automated methods of front recognition for climate studies: A case study in Southwest Western Australia, *Mon. Weather Rev.*, *142*(1), 343–363, doi:10.1175/MWR-D-12-00252.1.
Jayne, S. R., and J. Marotzke (2002), The oceanic eddy heat transport, *J. Phys. Oceanogr.*, *32*(12), 3328–3345, doi:10.1175/1520-0485(2002)032<3328:TOEHT>2.0.CO;2.
Le Traon, P.-Y., F. Nadal, and N. Ducet (1998), An improved mapping method of multisatellite altimeter data, *J. Atmos. Oceanic Technol.*, *15*(2), 522–534, doi:10.1175/1520-0426(1998)015<0522:AIMMOM>2.0.CO;2.
Mata, M. M., S. E. Wijffels, J. A. Church, and M. Tomczak (2006), Eddy shedding and energy conversions in the East Australian Current, *J. Geophys. Res.*, *111*, C09034, doi:10.1029/2006JC003592.
McDonald, N. R. (1998), The decay of cyclonic eddies by Rossby wave radiation, *J. Fluid Mech.*, *361*, 237–252, doi:10.1017/S0022112098008696.
Morrow, R. (2004), Divergent pathways of cyclonic and anti-cyclonic ocean eddies, *Geophys. Res. Lett.*, *31*, L24311, doi:10.1029/2004GL020974.
Nilsson, C., and G. Cresswell (1980), The formation and evolution of East Australian current warm-core eddies, *Prog. Oceanogr.*, *9*(3), 133–183, doi:10.1016/0079-6611(80)90008-7.
Nilsson, C. S., S. C. Andrews, and P. Scully-Power (1977), Observations of eddy formation off East Australia, *J. Phys. Oceanogr.*, *7*(5), 659–669, doi:10.1175/1520-0485(1977)007<0659:OOEFOE>2.0.CO;2.
Oke, P. R., G. B. Brassington, D. A. Griffin, and A. Schiller (2008), The Bluelink ocean data assimilation system (BODAS), *Ocean Modell.*, *21*(1–2), 46–70, doi:10.1016/j.ocemod.2007.11.002.
Oke, P. R., et al. (2013), Evaluation of a near-global eddy-resolving ocean model, *Geosci. Model Dev.*, *6*, 591–615, doi:10.5194/gmd-6-591-2013.
Oliveira, L. R., A. R. Piola, M. M. Mata, and I. D. Soares (2009), Brazil Current surface circulation and energetics observed from drifting buoys, *J. Geophys. Res.*, *114*, C10006, doi:10.1029/2008JC004900.
Pilo, G. S., M. M. Mata, and J. L. L. Azevedo (2015), Eddy surface properties and propagation at Southern Hemisphere western boundary current systems, *Ocean Sci.*, *11*(4), 629–641, doi:10.5194/os-11-629-2015.
Qiu, B., W. Miao, and P. Muller (1997), Propagation and decay of forced and free baroclinic Rossby waves in off-equatorial oceans, *J. Phys. Oceanogr.*, *27*(11), 2405–2417, doi:10.1175/1520-0485(1997)027<2405:PADOFA>2.0.CO;2.
Reynolds, R. W., T. M. Smith, C. Liu, D. B. Chelton, K. S. Casey, and M. G. Schlax (2007), Daily high-resolution-blended analyses for sea surface temperature, *J. Clim.*, *20*(22), 5473–5496, doi:10.1175/2007JCLI1824.1.
Ridgway, K. R., and J. R. Dunn (2003), Mesoscale structure of the mean East Australian Current system and its relationship with topography, *Prog. Oceanogr.*, *56*(2), 189–222, doi:10.1016/S0079-6611(03)00004-1.
Ridgway, K. R., and J. R. Dunn (2007), Observational evidence for a Southern Hemisphere oceanic supergyre, *Geophys. Res. Lett.*, *34*, L13612, doi:10.1029/2007GL030392.
Ridgway, K. R., and J. S. Godfrey (1997), Seasonal cycle of the East Australian Current, *J. Geophys. Res.*, *102*(C10), 22,921–22,936.
Ridgway, K. R., R. C. Coleman, R. J. Bailey, and P. Sutton (2008), Decadal variability of East Australian Current transport inferred from repeated high-density XBT transects, a CTD survey and satellite altimetry, *J. Geophys. Res.*, *113*, C08039, doi:10.1029/2007JC004664.
Rocha, C. B., I. C. A. Da Silveira, B. M. Castro, and J. A. M. Lima (2014), Vertical structure, energetics, and dynamics of the Brazil Current System at 22S-28S, *J. Geophys. Res. Oceans*, *119*, 52–69, doi:10.1002/2013JC009143.
Rykova, T., and P. R. Oke (2015), Recent freshening of the East Australian Current and its eddies, *Geophys. Res. Lett.*, *42*, doi:10.1002/2015GL066050, in press.
Schiller, A., P. Oke, G. Brassington, M. Entel, R. Fiedler, D. Griffin, and J. Mansbridge (2008), Eddy-resolving ocean circulation in the Asian-Australian region inferred from an ocean reanalysis effort, *Prog. Oceanogr.*, *76*(3), 334–365, doi:10.1016/j.pocean.2008.01.003.
Shi, C., and D. Nof (1994), The destruction of lenses and generation of wodons, *J. Phys. Oceanogr.*, *24*(6), 1120–1136, doi:10.1175/1520-0485(1994)024<1120:TDOLAG>2.0.CO;2.
Tranter, D. J., R. R. Parker, and G. R. Cresswell (1980), Are warm-core eddies unproductive?, *Nature*, *284*, 540–542, doi:10.1038/284540a0.
Tranter, D. J., G. S. Leech, and D. J. Vaudrey (1982), Biological significance of surface flooding in warm-core ocean eddies, *Nature*, *297*(5867), 572–574, doi:10.1038/297572a0.
Venaille, A., G. Vallis, and K. S. Smith (2011), Baroclinic turbulence in the ocean: Analysis with primitive equation and quasigeostrophic simulations, *J. Phys. Oceanogr.*, *41*, 1605–1623, doi:10.1175/JPO-D-10-05021.1.
Waterman, S., and S. R. Jayne (2011), Eddy-mean flow interactions in the along-stream development of a western boundary current jet: An idealized model study, *J. Phys. Oceanogr.*, *41*(4), 682–707, doi:10.1175/2010JPO4477.1.
Wunsch, C. (1997), The vertical partition of oceanic horizontal kinetic energy, *J. Phys. Oceanogr.*, *27*(8), 1770–1794.
Wunsch, C. (1999), Where do ocean eddy heat fluxes matter?, *J. Geophys. Res.*, *104*(C6), 13,235–13,249.
Wyrtki, B. (1960), The surface circulation in the coral and Tasman Seas, *Tech. Pap. 8, Div. Fish. Oceanogr.*, Cronulla, Australia.
Zhang, Z., W. Wang, and B. Qiu (2014), Oceanic mass transport by mesoscale eddies, *Science*, *345*(6194), 322–324, doi:10.1175/2459.1.